Tunneling dynamics of side chains and defects in proteins, polymer glasses, and OH-doped network glasses

Andreas Heuer[1] and Peter Neu[2]

[1] *Max-Planck Institut für Polymerforschung, Ackermannweg 10, D-55128 Mainz, Germany*

[2] *Department of Chemistry, Massachusetts Institute of Technology, Cambridge, Ma 02139*

Abstract

Simulations on a Lennard-Jones computer glass are performed to study effects arising from defects in glasses at low temperatures. The numerical analysis reveals that already a low concentration of defects may dramatically change the low temperature properties by giving rise to extrinsic double-well potentials (DWP's). The main characteristics of these extrinsic DWP's are (i) high barrier heights, (ii) high probability that a defect is indeed connected with an extrinsic DWP, (iii) highly localized dynamics around this defect, and (iv) smaller deformation potential coupling to phonons. Designing an extension of the Standard Tunneling Model (STM) which parametrizes this picture and comparing with ultrasound experiments on the wet network glass a-B_2O_3 shows that effects of OH-impurities are accurately accounted for. This model is then applied to organic polymer glasses and proteins. It is suggested that side groups may act similarly like doped impurities inasmuch as extrinsic DWP's are induced, which possess a distribution of barriers peaked around a high barrier height. This compares with the structurlessly distributed barrier heights of the intrinsic DWP's, which are associated with the backbone dynamics. It is shown that this picture is consistent with elastic measurements on polymers, and can explain anomalous nonlogarithmic line broadening recently observed in hole burning experiments in PMMA.

I. INTRODUCTION

Unlike simple systems such as atoms, nuclei or crystals, complex systems cannot be entirely characterized by the concept of a ground state and elementary excitations: The ground state of systems such as glasses, spin glasses or proteins is highly degenerate, and in place of energy levels or quasiparticles, we must speak in terms of a high-dimensional "energy landscape" in configuration space.[1−8] Basically the dynamics of the system is mapped on transitions between different basins of the energy landscape. Due to its complexity, this landscape is very rough and only very qualitative features are known about it. Experiments on myoglobin can be interpreted by saying that slightly different structures—conformational substate (CS), separated by high barriers—are organized in hierarchical tiers.[2,5,7] Glasslike behavior is also predicted for folded proteins (tertiary structure) by both theory and experiment.[4,9,10] Somewhat closer information about the multiple minimum energy landscape also comes from computer simulations on proteins, atomic clusters, and structural glasses.[4,11,12]

Whereas experiments at elevated temperatures (around the glass transition temperature T_g) are sensitive to the overall topology of the energy landscape, experiments far below T_g are sensitive to its fine structure. In the framework of the standard tunneling model (STM) this fine structure has been successfully characterized by using a statistical approach.[13,14] The STM explains many properties of glasses in the Kelvin regime. It assumes that via local rearrangements the system can switch between pairs of local energy minima. Formally, this corresponds to the dynamics of a particle in a double-well potential (DWP). At temperatures in the Kelvin regime the dynamics has to be described in quantum-mechanical terms. The resulting tunneling dynamics only involves the lowest two energy levels. Hence the DWP's act as two-level systems (TLS's). An important aspect of the STM is the assumption of a broad distribution of parameters characterizing DWP's and hence TLS's. In particular, this broad distribution implies that transition processes occur on a broad spectrum of time scales.

Most low temperature thermal, acoustic and optical properties of glasses can be explained in this picture.[15] However, recent hole burning experiments on a polymer glass (PMMA) in Haarer's group report a systematic disagreement with the STM.[16−18] The authors found a logarithmic time dependence with a crossover to an algebraic behavior after ca. 3 h. At the same time equivalent measurements have been performed on a protein (myoglobin) in Friedrich's group[19] with the result of almost no hole broadening up to 3 h and an algebraic time dependence thereafter. Very recently these results have been extended to longer waiting times.[20] Though the logarithmic behavior is in agreement with the STM, the algebraic behavior is not.

Apparently unrelated anomalies can be observed in sound attenuation experiments. In undiluted network glasses (SiO_2, GeO_2) a single relaxation peak appears around 50 K which is consistent with a broad distribution of DWP's.[21−23] However, an additional dilution with OH-impurities gives rise to the existence of a second relaxation peak at higher temperatures.[24,22] Specific mechanisms have been proposed giving rise to DWP's connected with the OH-impurities.[25]

Interestingly, sound attenuation measurements on various polymers also show an additional strong increase at temperatures above $\sim 30 - 50$ K.[26−30] Different absorption peaks— labelled by Greek letters $(\alpha, \beta, \gamma, \delta)$ in appearance of decreasing temperature—have been observed in the temperature regime between $\sim$ 30 K and room temperature.[26,27] Usually, the low temperature peaks (δ, γ, β) are attributed to side chain motions, which perform thermally activated reorientation processes even far below T_g.[26−28,31]

This similarity between sound absorption in OH-doped network glasses and in polymer glasses may justify to think of side chain as "defects", because both hydroxcyl groups and side groups give rise to well-defined localized DWP's. Thus one may ask the question whether the statistical approach of the STM still holds as soon as a significant fraction of DWP's is related to the dynamics of some well-defined defects.

The conjecture we want to investigate in this paper is: (1) the existence of minority components of different structure (impurities as compared to the network or side groups as

compared to the main chain) give rise to additional localized dynamical degrees of freedom; (2) associated with these degrees of freedom are induced or *extrinsic DWP's* which possess a nonuniversal, i.e., different from the STM, distribution of parameters; (3) these extrinsic DWP's cause a second absorption peak of sound at higher temperatures and a nonlogarithmic hole broadening at ultralong time scales. In what follows both OH-impurities and side groups will be referred to as defects.

Rather than just postulating the nonuniversal properties of defects, we first show via computer simulations of a simple model glass that the presence of defects indeed has dramatic consequences for the distribution of DWP's. We choose a binary Lennard-Jones (LJ) glass which has been tested in previous simulations and has proven to confirm the assumptions of the STM.[32] The LJ parameters are chosen to represent NiP. To this LJ glass we add "defects" (minority component) in form of a third LJ particle. The size of the defect will be controlled via its LJ parameters by a variable interaction length. The main finding of these simulations is that, in case that the minority component is somewhat smaller than the original glass components, they give rise to additional or extrinsic DWP's with high energy barriers whereas in case of large defects no extrinsic DWP's occur. The existence of small particles also has some impact on the *intrinsic* DWP's which are connected with the majority component. Although these results might not be representative for all glasses, one can speculate that as a general result the distribution of DWP's in systems with defects can be viewed to additionally comprise typical high barriers. Based on this observation, we design a model which extends the STM, and compare to experiments on OH-diluted network glasses, polymer glasses and proteins.

The outline of this paper is as follows: In Sec. II, we describe the simulation method and present the results; in Sec. III, an extension of the tunneling model is proposed taking into account an additional contribution of DWP's with high barrier heights; in Sec. IV, we compare with experiment, and, in Sec. V, we conclude. Mathematical details are relegated to the Appendix in order not to interrupt the main flow of the paper.

II. SIMULATIONS

A. Model for the computer glass

The model LJ-type glass has been adapted from the work of Weber and Stillinger[33] and is devised to represent the binary glass former NiP. The system contains 80% type 1 (Ni) and 20% type 2 (P) particles. The interaction is pairwise and reads

$$
V_{ij} = \begin{cases} A_{ij}[(\alpha_{ij}r/\sigma)^{-12} - 1]\exp[-\sigma/(a - \alpha_{ij}r)], & \text{for} \quad 0 < \alpha_{ij}r \le a \\ \\ 0 & \text{else} \end{cases} \tag{1}
$$

with $a = 1.652\,\sigma$ where $\sigma = 2.2$ Å is the unit length. Values for A_{ij} and α_{ij} are $A_{11} = 8200$ K, $\alpha_{11} = 1.0$ (Ni-Ni), $A_{12} = 1.5\,A_{11}, \alpha_{12} = 1.05$ (Ni-P), $A_{22} = 0.5\,A_{11}$, and $\alpha_{22} = 1.13$ (P-P). The mass density ρ_0 is 8348 kg/m^3. We have simulated systems with $N = 150$ particles and use periodic boundary conditions. We have checked that within statistical errors a simulation with $N = 500$ particles yields identical results. The equilibrium distance between two particles of type i and j is given by parameters $2^{1/6}\sigma/\alpha_{ij}$. In extension to the above model we include a single particle which we formally denote type 3 particle. Its potential parameters are chosen as $\alpha_{i3} = \alpha$ and $A_{i3} = A_{11}$. The value of α determines the equilibrium distance between this particle and the rest of the glass and hence characterizes the effective size of this particle. The simulations have been performed in the range $0.7 \le \alpha \le 1.6$. Of course, one expects that for $\alpha \sim 1$ this particle basically behaves like the rest of the glass for which 96% of all pair potentials are characterized by $\alpha = 1$ or $\alpha = 1.05$.

B. Simulation method

In previous work Heuer and Silbey developed a systematic search algorithm for DWP's.[32] Starting from some $T = 0$ configuration of a glass the idea is to search the energy landscape around some local minimum for a second local minimum. This pair of minima can be viewed as a DWP. The full cooperativity of the transition between both minima is taken

into account. In general all particles will be involved in the transfer between both minima. Let d_i denote the transfer distance of the i-th particle. The total distance of both minima in configuration space can then be expressed as

$$d^2 \equiv \sum_i \vec{d}_i^2. \tag{2}$$

The algorithm takes advantages of the observation that the existence of DWP's is related to a somewhat localized motion of particles. For different initial $T = 0$ configurations we analyzed the region around the defect and checked whether we can find a DWP close to this defect. This is achieved in three steps. In a first step we choose the defect particle as well as its 15 nearest neighbors. Then in a second step we minimize the potential energy via some simulated annealing routine by moving the 16 selected particles such that the distance in configuration space to the original local minimum is $d_0 = 0.4\,\sigma$. By this condition we avoid that the system just moves back to the original minimum. Finally, we relax the whole system to find a new local minimum. In case that close to the original minimum there exists a second minimum the algorithm will likely find this new minimum. A careful analysis for this choice of d_0 has shown that DWP's with $d_0 < d < \sigma$ are systematically found by this algorithm. Anyhow, the fraction of DWP's with $d < 0.4\,\sigma$ is very small. In present work we restrict ourselves to DWP's with d in this range. For the binary LJ glass it turned out that there exist one DWP per 100 particles. Hence in a small region around the defect one expects at most a single DWP. Further details about this algorithm as well as a discussion of its limitations can be found in Ref. 32.

We wish to distinguish the properties of extrinsic and intrinsic DWP's. For this purpose, we determine for all DWP's which particle moves most during the transition between both local energy minima and denote this distance by d_s. If this particle is the defect we denote this DWP extrinsic, otherwise intrinsic. Finally the effective mass is defined via

$$p \equiv d^2/d_s^2 \geq 1. \tag{3}$$

The value of p is a measure for the number of particles which are basically involved in the formation of the DWP. Finally, the potential height of a DWP is found by an explicit search

for the saddle point. The present analysis is based on the analysis of approximately 3000 independent initial configurations.

C. Results of the simulations

First we determine the probability that a DWP exists close to the defect. In Fig. 1 the probability is shown that the algorithm, described in Sec. IIA, finds an extrinsic DWP. One can see that the number of extrinsic defects dramatically increases for large values of α. For the smallest particles analyzed in our simulation runs nearly 80% of all defects are connected with a DWP. Of course, this number has to be viewed as a lower limit since it is possible that our algorithm may miss some DWP's. However, this already large number shows that the algorithm works realibly. For $\alpha = 1$ the defect is basically identically to the rest of the glass. Hence the probability at $\alpha = 1$ has to be identical to the probability (normalized per particle) to find a DWP in the whole glass. The present result agrees with the already above-mentioned finding of Ref. 32 that on average one DWP exists per 100 particles. For us it was very surprising that already for $\alpha = 1.2$ a significant number of extrinsic DWP's can be observed. Hence only small differences between defect and structural glass seem to strongly enhance the probability for the formation of a DWP. For $\alpha = 0.7$ no extrinsic DWP has been found. A huge particle is locked in a cage formed by the surrounding small particles without a chance to escape.

In Fig. 1 the probability to find intrinsic DWP's is displayed, too. Originally, the simulation yields the probability that there exists an intrinsic DWP's having a significant spatial overlap with the initially selected particle cluster; see the description of the algorithm above. For $\alpha = 1$ this probability is larger than the probability for the formation of extrinsic DWP's although no difference between intrinsic and extrinsic DWP's should exist. The reason is trivially related to the asymmetry in the definition of intrinsic and extrinsic DWP's. For $\alpha = 1$ the ratio of the number of intrinsic and extrinsic DWP's should be close to the number of initially selected particles around the defect (here: 15 particles). This unwanted

statistical effect can be removed by scaling the probability of formation of intrinsic DWP's such that for $\alpha = 1$ this probability is equal to that of the formation of extrinsic DWP's. This allows a direct comparison between intrinsic and extrinsic DWP's. All data in Fig. 1 for the intrinsic DWP's are scaled in this way. Interestingly, the number of intrinsic DWP's close to the defect strongly depends on the size of the defect. The number is largest for $\alpha \approx 1$, but strongly decreases for larger or smaller defects. We interpret this observation as follows: for α very different to unity the defect does not participate in the dynamics of the glass because it does not move at all (small α) or because it only moves by itself (large α). Hence from the viewpoint of the glass particles there exists an "alien element" which forms a barrier for the surrounding particles. Thus close to the defect the degrees of freedom and hence the chance to form a DWP are significantly reduced. Only for $\alpha \approx 1$ this effect is irrelevant since the defect may simply participate in the dynamics.

In order to characterize the nature of the extrinsic DWP's somewhat closer, we plot the average effective mass p of the DWP's in dependence of α; see Fig. 2. One observes a transition from cooperative to strictly localized dynamics. Already for $\alpha = 1.2$ the effective mass of extrinsic DWP's starts to decrease. For $\alpha = 1.6$ the extrinsic DWP's are related to motions of the defect alone. In the limit of very small particles this result could have been expected. Basically the defect jumps between different interstitial positions formed by a fixed environment. It is likely that for large α a defect has more than one direction in order to find a second minimum. From the present simulations this suggestion cannot be quantified.

In Fig. 3, we plot the distribution of barrier heights of intrinsic DWP's with the presence of a close-by defect as well as the distribution for extrinsic DWP's related to $\alpha = 1.6$. In both cases a broad distribution of barrier heights is observed reflecting the statistical nature of the formation process of a DWP. However, obviously the extrinsic defects in case of small defects are significantly shifted to higher potential heights. This is quantified in Fig. 4, where we plot the average barrier height V in dependence of α. In agreement with Fig. 3, one observes a strong increase of the value of the average potential height with α. As

already discussed in Ref. 32, the ability to cooperative motion, i.e., a large effective mass p, tends to decrease the necessary energy changes along the way between both minima of a DWP. In the opposite limit $p = 1$ a single particle has to move by itself, hence experiencing strong resistance by the environment leading to a larger value of the barrier height. This general statement is again confirmed by the observed correlation between the effective mass and the average barrier height; compare Figs. 2 and 4.

Finally, in Fig. 5, we show the value of the deformation potential γ, normalized such that $\gamma(\alpha = 1) = 1$. The theoretical basis for this calculation can be found in Ref. 34. The deformation potential decreases with increasing α. This effect can easily be explained. The number of nearest neighbors of the defect strongly depends on its size and decreases with decreasing size. This can be easily visualized for a regular hexagonal lattice in two dimensions where particles on interstitial sites are surrounded by three particles whereas the coordination number of a regular lattice site is six. Since the deformation potential is related to the interaction of the defect with the environment it is not surprising that the deformation potential strongly depends on the number of nearest neighbors.

III. EXTENSION OF THE TUNNELING MODEL

In the STM it is assumed that the asymmetry energy between two wells, ϵ, and the tunneling parameter, $\lambda = (d/\hbar)\sqrt{2mV}$, are uniformly distributed over a wide range,

$$P(\lambda, \epsilon)\, d\lambda\, d\epsilon = P_0\, d\lambda\, d\epsilon \tag{4}$$

with a constant $P_0 \approx 10^{44} - 10^{46}$ J^{-1} m^{-3} for most glasses. Here, m represents the mass of the tunneling unit, and d the distance between the minima of the double-well potential. The tunneling parameter is related to the tunneling amplitude, Δ, through a WKB relation

$$\Delta = \hbar\omega_0\, e^{-\lambda}, \tag{5}$$

where $\hbar\omega_0$ is essentially the zero-point energy, and to the one-phonon relaxation rate by

8

$$R(E, \lambda) = R_{\max}(E) \, e^{-2(\lambda - \lambda_{\min}(E))} \tag{6}$$

where

$$\lambda_{\min}(E) = \log(\hbar \omega_0 / E). \tag{7}$$

The detailed form of the maximum rate, $R_{\max}(E)$, at fixed TLS-energy, $E = \sqrt{\Delta^2 + \epsilon^2}$, depends on the spectral density of vibrational modes in the energy landscape. Usually, a deformation potential coupling, with parameter γ, to a Debye-spectral density, $J(\omega) \propto \omega^3$, is imposed. The one-phonon rate then reads $R = (\Delta/E)^2 J(E/\hbar) \coth(E/2k_B T)$ which together with (5) and (6) provides

$$R_{\max}(E) = cT^3 x^3 \coth x \, , \tag{8}$$

where $x = E/2k_B T$ and $c = \gamma^2 (2k_B)^3 / 2\pi \hbar^4 \varrho v^5$. Here, ϱ is the mass density and v the averaged sound velocity. The ensuing hyperpolic distribution for Δ and R, $P(\epsilon, \Delta) = P_0/\Delta$ or $(\epsilon/E)P(E, R) = P_0/2R$, explains in particular the broad distribution of relaxation processes in glasses on a logarithmic time scale.

The simulations suggest to extend the tunneling model by adding a second peak for a glass with additional defects (OH-groups) or a polymer glass (side chain motion) [cf. Fig. 1]. In order to restrict ourselves to a minimum set of new parameters, we only characterize this second peak by its mean value and its width in the following model:

$$P(\epsilon, \lambda) = P_0 \, e^{-(\lambda - \lambda_0)^2 / 2\sigma_0^2} \; + \; P_1 \, e^{-(\lambda - \lambda_1)^2 / 2\sigma_1^2} \, , \qquad \lambda \geq \lambda_{\min}(E), \tag{9}$$

where P_0 and P_1 weights the density of the intrinsic and extrinsic TLS's. By formulating the new distribution for the tunneling parameter, λ, we additionally assume some relation between the potential height V and the distance between the two minima of the DWP, d. The standard assumption is $V \propto d^2$. For $P_1 = 0$ and $\sigma_0 \gg 1$ the standard model emerges.[13,14] The parameter λ_0 determines the most probable tunneling matrix element. For all practical applications this parameter in irrelevant and will be set to zero hereafter. A model including only the first term has previously been used by Jankowiak and Small.[35] As we will see below,

a combination of both terms is needed in order to explain several experiments consistently. These authors have also emphasized the importance of extrinsic TLS, which they attribute to the presence of the chromophores in the probe.

The ensuing distribution in $\Delta = \hbar\omega_0\, e^{-\lambda}$ then reads after neglecting terms depending on $(1/2\sigma_0^2)\log(\hbar\omega_0/\Delta) \ll 1$

$$P(\epsilon,\Delta) = \frac{P_0}{\Delta} + \frac{P_1'\,(\hbar\omega_0)^{\nu(\Delta)}}{\Delta^{1+\nu(\Delta)}}\ , \tag{10}$$

where $P_1' = P_1 e^{-\lambda_1^2/2\sigma_1^2}$ and

$$\nu(\Delta) = \frac{\lambda_1}{\sigma_1^2} - \frac{1}{2\sigma_1^2}\,\log(\hbar\omega_0/\Delta). \tag{11}$$

Identifying σ_0 with the parameter $\lambda_{\max}$ of the STM, one deduces that $10 \lesssim \sigma_0 \lesssim 30$. The value of P_1 depends on the concentration of the defects. For a typical concentration of OH-groups in network glasses, one expects $P_1 \lesssim P_0$. In polymer glasses, however, the number of extrinsic DWP's can be larger because of the large number of side chains. If every side chain contributes one extrinsic DWP, and if only one out of ~ 100 monomers of the backbone forms an intrinsic DWP[32], we find as an upper bound that $P_1 \lesssim 100\, P_0$. More difficult is the estimation of mean value and the width of the second peak. For $\alpha = 1.6$ one observed numerically an average value of $d \approx 0.6\,\sigma$. Together with the average potential height $V_{av} = 800$ K and using the average atomic mass of NiP one may estimate $\lambda_1 \sim 35$ and $\sigma_1 \sim 25$. However, for any realistic applications λ_1 (or V_{av}) and σ_1 depend on the exact nature of the defects and hence should be treated as adjustable parameters. Due to the observation of several absorption maxima below the glass transition temperature,[26,27] a more realistic model should contain more than one additional peak in the distribution of barrier heights. Since we are interested in low temperature properties, it is sufficient to include only the lowerst addition barrier peak in our model.

IV. COMPARISON TO EXPERIMENT

A. Sound attenuation in OH-doped network glasses and polymers

A possible method to measure sound absorption is to clamp a small glassy plate on one end and to drive it electrostatically to forced vibrations on its free end, the so-called vibrating reed technique.[21–23] The measurement of the resonance frequency and the amplitude of the plate then determines the acoustic loss and the variation of the sound velocity.

Measurements of the elastic properties of glasses—for example the internal friction, Q^{-1}—have proven to be a powerful method for the study of tunneling states below ~ 5 K, where it is assumed that relaxation occurs with the one-phonon rate (6). At higher temperatures, typically between 10 K and room temperature, the elastic measurements provide information about the distribution of potential barrier heights for thermally activated reorientations,[36]

$$\tau = \tau_0 \, e^{V/k_B T} \tag{12}$$

with $\tau_0 \approx 10^{-13}$ s, of atoms and molecules. Assuming a simple oscillator model for the individual wells of a DWP, we have $V \propto d^2$ and

$$\Delta = \frac{2E_0}{\pi} e^{-\lambda}, \tag{13}$$

where E_0 is the zero-point energy of the oscillator, and

$$\lambda = \frac{V}{E_0}. \tag{14}$$

With this, the distribution (9) can be rewritten yielding

$$P(\epsilon, V) = \frac{P_0}{E_0} e^{-(V-V_0)^2/2\widetilde{\sigma}_0^2} + \frac{P_1}{E_0} e^{-(V-V_1)^2/2\widetilde{\sigma}_1^2} \tag{15}$$

with $V_i = \lambda_i E_0$ and $\widetilde{\sigma}_i = \sigma_i E_0$, and the internal friction, Q^{-1}, can be calculated with the formalism developed in Ref. 21.

Comparing the data for dry and wet a-B$_2$O$_3$ in Figs. 7 and 8 of Ref. 22, one clearly sees that the sound absorption is strongly effected by the presence of OH-impurities. For the dry sample a broad absorption peak is observed around ~ 50 K, while for the wet

sample a shoulder between 30 and 80 K is followed by a narrow peak at ~ 160 K. Similar observations have been made in Ref. 24, where the dry a-B_2O_3 sample provided one broad peak whereas the wet sample showed two maxima. The authors in these references concluded that intrinsic DWP's cause a loss peak at lower and OH-induced, i.e., extrinsic DWP's a peak at higher temperatures. Independent of any theoretical framework, these experiments directly indicates that the barrier heights of these OH-related DWP's must be higher than those of DWP's related to the glass itself. Furthermore, the mere fact that approximately 1% OH-content can have such a significant influence on the relaxation properties shows that OH-defects have to be very efficient in prompting the formation of DWP's.

In Fig. 6, we have plotted the internal friction data of wet a-B_2O_3 sample together with a fit from our model (15) and[37]

$$Q^{-1} = \frac{\gamma^2}{\varrho v^2 k_B T} \int d\epsilon \int dV \; P(\epsilon, V) \; \text{sech}^2(\epsilon/2k_B T) \; \frac{\omega \tau}{1 + (\omega \tau)^2}, \qquad (16)$$

where τ is given by the one-phonon rate (6) or the Arrhenius rate (12) depending on whether the temperature is in/below the plateau regime or above, respectively. The data are from Ref. 22. The solid line shows the contribution of intrinsic and extrinsic DWP's; the dashed line the contribution of intrinsic DWP's. The parameter values are given in the figure caption. We see that elastic measurements are a powerful tool to determine the barrier heights distribution, and that our computer simulation based model (15) accounts well for the influence of OH-defects in network glasses.

Let us now discuss the elastic properties of polymers.

Nittke et al.[30] have recently measured the low temperature (< 50 K) elastic properties of the polymer glasses polymethylmethacrylate (PMMA) and polystyrene (PS) at $\omega = 2\pi \times 240$, 535 and 3200 Hz, following earlier measurements by Federle and Hunklinger[38] at $\omega = 2\pi \times 15$ MHz and Geis, Kasper, and Hunklinger[29] at $\omega = 2\pi \times 430$ Hz in PMMA. In the latter work, also the high temperature absorption between 50 and 300 K has been measured following previous work, cf. Refs. 26–28. Below ~ 30 K the acoustic loss of PMMA and PS shows the typical temperature dependence of network glasses like SiO_2: the

12

plateau merges in the thermally actived relaxation peak around ~ 5 K. The missing first relaxation peak of the acoustic loss in PMMA at $\omega = 2\pi \times 535$ Hz (cf. Fig. 12 in Ref. 30 or Fig. 4 in Ref. 29) can well be explained by the low applied frequency $\omega/2\pi$ and a small value for the cutoff, $V_{\max}$, in the barrier distribution of the STM-states.[39] However, above ~ 30 K both polymers behave anomalously compared to (undoped) network glasses by exhibiting a strong increase in their acoustic loss. Early measurements show that this increase is characteristic for polymers and continues up to the glass transition temperature with various (δ, γ, β) relaxation peaks superimposed to it.[26,27] Recently, multidimensional NMR measurements have proven that the molecular origin of the β relaxation in PMMA at 330 K (10 Hz) is a large-amplitude flip of the methacrylate side group around the C–C bond and a concomitant main chain torsion.[31] From the evidence at present available the nature of the groups responsible for the low temperature δ, γ peaks which have been observed in different polymers is less clear, however, they have traditionally been attributed to thermally activated rotation of sub groups within the side chains. Examples are the n-alkyloxycarbonyl side group rotations of the polymethacrylates, see Figs. 3 and 4 in Ref. 27. In PMMA these side groups do not exist and absorption peaks observed at temperatures below the β peak[29] are thought to be due to the presence of small amounts of dibutylphtalate (DBP)—a plasticizer—or higher polymethylacrylate esters. Studies on purified samples, which revealed a pure exponetial increase, $Q^{-1} \propto e^{aT}$, between ~ 30 and ~ 300 K, support this interpretation.[26,27] However, even with a broad distribution, it is not clear whether the exponential increase is connected with the β process. It is conceivable that further molecular dynamics occurs in the intermediate temperature regime.

In any case we learn from these experiments that (1) the similarity between sound absorption in OH-doped network glasses and in polymer glasses may justify to think of side chain as "defects", because both hydroxcyl groups and side groups give rise to well-defined localized motion within DWP's with high activation barriers, and thus constitute additional degrees of freedom; (2) the energy landscape of polymers is structured at higher barrier heights: in addition to the uniformly distributed low barriers being responsible for the

plateau region below ~ 6 K, several tiers of high barriers with typical activation energies can exist depending on the chemical compound of the polymer.

B. Hole burning in polymer glasses and proteins on ultralong time scales

In a hole burning experiment the probe is doped with a large number of guest molecules having resonance frequencies in the optical range. Due to the disordered structure of the host each chromophore experiences a slightly different environment which detunes its resonance frequency; the absorption line becomes inhomogeneously broadened, accordingly. A fraction of these chromophores is photochemically or photophysically removed from the absorption line by laser irradiation. The inhomogeneous line then shows a narrow hole at the laser irradiation frequency. Each chromophore is interacting with local rearrangements of atoms in the host which conveniently can be described in the TLS picture. As a result, the resonance frequency of the guest molecule performs spectral jumps and its linewidth becomes broadenend. This process, which is called "spectral diffusion", results in a partial refillment and, thereby, in a broadening of the hole. Hence, the time dependence of the hole width is a mirror of the relaxation processes in the host, and, accordingly, a tool to investigate the local dynamics of the host. In proteins and glasses the results can be interpreted by the concept of an energy landscape.

In recent years this technique has been used extensively by various groups on glasses and proteins.[8,16−20,40−44] Most measurements on glasses for times $t \le 3$ h confirm the STM, which predicts according to $(\epsilon/E)P(E,R) = P_0/2R$ and

$$\Delta\Gamma(t) = \frac{\pi^2}{3\hbar}\langle C\rangle \int dE \operatorname{sech}^2 \frac{E}{2k_BT} \int dR\,\frac{\epsilon}{E}\,P(E,R)\left(e^{-Rt_0} - e^{-Rt}\right) \tag{17}$$

a logarithmic growth

$$\Delta\Gamma(t) \equiv \Gamma(t) - \Gamma(t_0) = \frac{\pi^2}{3\hbar}P_0\langle C\rangle k_BT\,\log(t/t_0) \tag{18}$$

of the hole width after some reference time t_0.[42,45−48] Here, $\langle C\rangle$ is the chromophore-TLS coupling strength. This accords with the broad distribution of relaxation times on logarithmic

14

time scales.

Recently, Haarer and coworker[16–18] have performed hole burning on purified PMMA at 0.5, 1 and 2 K up to extremely long times (from 10 s to 10 days), see data points in Fig. 7. They found a $\log(t)$-dependence up to ca. 3 h, but a $\sqrt{t}$-behavior between 3 h and 10 days. Furthermore, Friedrich and coworker[19,20] have performed equivalent measurements on proteins at 100 mK and 4 K. In Ref. 19, these authors did photochemical hole burning on a glycerol/water glass over 44 h with and without the protein myoglobin doped into the sample, see data points in Fig. 8. Recently, they also studied the protein cytochrome c in a glycerol/dimethylformamide glass[20] for 300 h, see data points in Fig. 9. The result was: (i) spectral diffusion broadening is always less in the protein than in the glass; (ii) the glass showed a logarithmic time dependence within the first 3 h, while there was practically no relaxation in the protein over this period; (iii) after about 3 h there is a strong nonlogarithmic increase in the line broadening for both the glass and the protein; (iv) contrary to the glass, the protein showed no aging effect indicating a gap in the relaxation rate between 1 s and ~ 3 h. The protein and the glass data could be fitted with an empirical *ad hoc* ansatz for the distribution function

$$P(\epsilon, \Delta) = P_0 \left[\frac{1}{\Delta} + \frac{A}{\Delta^2} \right] , \qquad A = \text{constant}, \tag{19}$$

resulting in a growth composed of a superposition of a $\log(t)$- and a $\sqrt{t}$-term. For the 0.5 and 1 K data in PMMA a single consistent parameter set with $A/k_B = 10^{-7}$ K has been used.[16,17] For the 2 K data in PMMA, however, a 60% smaller value for the weight parameter A was needed.[18] For the protein data the question rises whether there is a $\log(t)$-term or not as the data can already be reproduced by the $\sqrt{t}$-term. This observation motivated the authors in Ref. 20 to discuss a possible alternative interpretation of the nonlogarithmic dynamics which is related to classical diffusion in the energy landscape.

In both experiments the distribution function (19) has been motivated by recent publications focusing on the interaction of TLS's in glasses,[49–51] in particular by the scenario of coherently coupled pairs of TLS's, which was invented by Burin and Kagan.[51] In this

formulation the second term in (19) stems from pairs of single TLS's which are coupled by a (resonant) up-down transition.[51,52] If the single TLS's are distributed as in the STM [first term in Eq. (19)], a $1/\Delta^2$-distribution emerges for the pairs. In Ref. 52, a quantitative test of this picture has been performed with the conclusion that this strongly modified TLS model could, in principle, explain the deviation from the $\log(t)$-dynamics. At higher temperatures pairs are expected to break up due to thermal fluctuations which destroy the coherence of the coupling. It has been suggested that this is the physical reason for the decrease of the weight factor A seen in the PMMA data at 2 K.[18]

In the following, we will propose an alternative explanation, which is motivated by the acoustic measurement on polymers, and has no restriction towards higher temperatures.

Instead of considering TLS-flip-flop processes as the physical cause of spectral diffusion, we take barrier crossings events. On the time scale of seconds and larger, both picture are of course equivalent due to the big ratio ϵ/Δ of the relevant TLS or DWP's. We assume that at 1 K the barrier crossing process occurs via tunneling with the one-phonon rate, Eqs. (6)–(8), and consider the tunneling parameter λ, which in the simple oscillator model (14) is equivalent to the barrier height V. Because of the observation that the broadening significantly increases at 1 K between $t_c = 10^3$ and 10^4 s, and that the distribution $P(\Delta) \propto 1/\Delta^2$ well accounts for this phenomenon, we learn that the distribution $P(\lambda)$ increase exponentially around some value $\lambda_c \gg 1$. We may estimate this value from the relation $R(1\,\mathrm{K})t_c \sim 1$ which provides with $R_{\max}(1\,\mathrm{K}) \approx 10^{10}$ s^{-1} that $\lambda_c - \lambda_{\min}(1\,\mathrm{K}) \approx 15$. A natural way to interpret this increase in λ is to assume that *the energy landscape of a polymer glass is not structureless, but that it comprises high barriers in addition to structurelessly distributed lower barriers within each basin*—as observed in the acoustic experiments on polymer glasses. This is the picture which Frauenfelder suggested for the energy landscape of proteins.[3,5,6] We may identify transitions between deep basins with degrees of freedom (rotations or switching) located at the side chains of the polymer glass or protein. The STM-like states may be associated with the more collective dynamics along the backbone or the network. One might think that already the backbone dynamics of polymers gives rise to dynamics with high bar-

rier heights, since this dynamics is related to conformational transitions. However, it has been shown for some polymers that conformational transitions occur on the same time scale as the α relaxation and thus can be neglected at temperatures far below T_g.[53] The reason is that conformational transitions involve highly cooperative dynamics in contrast to more localized processes we are here interested in and which are still active below T_g.

The difference between protein and glass then simply lies in the amount of disorder and organization in the energy landscape. Though deep basins separated by saddle points exist in both materials, in proteins the distribution of small (STM-like) barriers in the basins is restricted to smaller values, i.e., $\sigma_0(\text{protein}) \ll \sigma_0(\text{glass})$, or, more likely, itself composed of many well-separated distributions yielding the hierarchical picture of Frauenfelder with STM-like states on the lowest tier. Indeed, recent stimulated echo experiments by Thorn Leeson and Wiersma can be interpreted in this way.[7] Hence, whereas many different tiers can exist in proteins, the glass is less organized: the structurelessly distributed STM-states extend to much higher barriers, and only the passing from one basin to the next gives rise to an (in the sense of the STM) anomalous behavoir. Hence, we suggest a connection between the low temperature ($\overset{<}{\sim} 100$ K) relaxation peaks observed in elastic measurements with the nonlogarithmic line broadening observed in spectral hole burning after $10^3 - 10^4$ s in the temperature regime around 1 K. A crossing of barriers as high as $\overset{<}{\sim} 1000$ K by *tunneling* at 1 K is only possible because of the extreme long waiting time of $10^3 - 10^6$ s. At higher temperatures ($\overset{>}{\sim} 5$ K) the one-phonon rate should gradually be replaced by the Arrhenius rate (12), which will change the temperature dependence, but not the time dependence of the hole broadening.

The simplest way to quantify our ideas is to calculate the hole broadening from Eq. (9) and compare with the experimental data of Refs. 16–18 and 19,20. In the Appendix we give details of the derivation. We find for typical values of the shortest time a hole can be read, $t_0 \sim 1$ s,

$$\Delta\Gamma(t) = \frac{\pi^2}{3\hbar}\langle C \rangle \, k_B T \left[\, P_0 \sigma_0 \sqrt{2\pi} \, f^{(1)}(t) \; + \; P_1 \sigma_1 \sqrt{2\pi} \, f^{(2)}(t) \, \right], \tag{20}$$

where

$$f^{(1)}(t) = \text{erf}\left(\frac{(1/2)\log(KTt)}{\sigma_0\sqrt{2}}\right) - \text{erf}\left(\frac{(1/2)\log(KTt_0)}{\sigma_0\sqrt{2}}\right), \tag{21}$$

$$f^{(2)}(t) = \text{erfc}\left(\frac{\lambda_1 - (1/2)\log(KTt)}{\sigma_1\sqrt{2}}\right) - \text{erfc}\left(\frac{\lambda_1 - (1/2)\log(KTt_0)}{\sigma_1\sqrt{2}}\right). \tag{22}$$

Here, $\text{erf}(x)$ ($\text{erfc}(x)$) is the (complementary) error function, and K has been defined in Eq. (A.6). The first term yields with $\text{erf}(z) \overset{z \ll 1}{\longrightarrow} (2/\sqrt{\pi})z$ in leading order in $(1/\sigma_0)$ the standard result (18). If the barrier crossing is thermally activated with rate $\tau^{-1} = \tau_0^{-1}e^{-V/k_BT}$, one easily finds that within the simple oscillator model (14) and (15)

$$f^{(1)}(t) = \text{erf}\left(\frac{k_BT\log(t/\tau_0)}{\widetilde{\sigma}_0\sqrt{2}}\right) - \text{erf}\left(\frac{k_BT\log(t_0/\tau_0)}{\widetilde{\sigma}_0\sqrt{2}}\right), \tag{23}$$

$$f^{(2)}(t) = \text{erfc}\left(\frac{V_1 - k_BT\log(t/\tau_0)}{\widetilde{\sigma}_1\sqrt{2}}\right) - \text{erfc}\left(\frac{V_1 - k_BT\log(t_0/\tau_0)}{\widetilde{\sigma}_1\sqrt{2}}\right), \tag{24}$$

with $\widetilde{\sigma}_i = E_0\sigma_i$, which, as mentioned above, changes the temperature but not the time dependence of the line width.

In Figs. 7 to 9, we compare Eq. (20) - (22) with the experimental data for PMMA, glycerol/water glass and myoglobin, and cytochrome, respectively. The parameter values are given in Table I and II. In the glasses PMMA and glycerol/water glass, logarithmic line broadening occurs below $\sim 10^4$ s, as predicted by the STM. The experimentally detected algebraic $\sqrt{t}$-time dependence applies approximately between 10^4 and 10^6 s. As is clearly demonstrated in Fig. 7, it arises from a superposition of the two terms in Eq. (20). Hence, the experimentally found exponent $1/2$ has no physical significance in this model. The protein data can be fitted without a $\log(t)$-term (i.e., $P_0 = 0$) as the dashed lines in Fig. 8 and 9 illustrate. In any case the contribution of the $\log(t)$-term is very small as can be inferred from the dash-dotted curve in Fig. 9. This is consistent with the absence of aging observed in Ref. 20 (see data points corresponding to different equilibration times in Fig. 9), which indicates a gap in the distribution of relaxation times between ~ 1 s and 3 h. The hole broadening of glycerol/water glass and myoglobin embedded in the glycerol/water glass could not be fitted with the same set of parameters, which clearly indicates the protein

18

comprises itself TLS's which dephase the chromophore. The numerical values for K, $P_0\langle C\rangle$ and σ_0 are in the range known from other experiments. The numerical values for the new parameters λ_1, σ_1, and P_1/P_0 lie well within the range we estimated from the numerical simulations. Using the parameter set for PMMA in Table I for the acoustic measurement of Refs. 29,30 is difficult because we do not know the exact relation between V and λ. However, assuming $E_0(\text{PMMA}) \sim 10-20\,\text{K}$ we see that the increase in the sound absorption in PMMA should be at a lower temperature than for the OH-doped Boroxid glass—as observed in the experiment.

C. Comparison of elastic and optical properties of PMMA and experimental test

Our picture of a structured barrier heights distribution seems to be consistent with elastic and optical measurements on polymers. However, in PMMA the puzzle remains that purified samples contain no sound absorption peak in the temperature regime below the β peak (~ 330 K). Hence, no peaks in the barrier heights distribution seem to exist in the regime below say 1000 K, which is the relevant order of magnitude to obtain a nonlogarithmic line broadening between 10^4 and 10^6 s. However, one must exercise caution since the experimentally observed exponential increase in the acoustic loss between 20 and 300 K can hide different dynamic molecular processes. Furthermore, in principle, our simulations show that *any* impurity can generate such an additional peak in the barrier distribution, and that defects are very effective in prompting external DWP's. A very low concentration of defects is sufficient to have dramatic effects. Hence, it is possible that the presence of impurities such as exchange gas atoms, monomers, fragments, hydrocyl groups, etc., is reponsible for this process. Also, it is unclear what the role of the chromophores may be, although the observation of a logarithmic line broadening in proteins, where the chromophore only replaces a group of a *similar* structure (i.e., does not change the local configuration of the protein), makes the presence of the chromophore a doubtful cause of the nonlogarithmic line broadening. Furthermore, our simulation did not show any additional peaks in the barrier

heights distribution function upon adding *large* impurities to the LJ-glass.

There are several possibilities for an experimental test whether the physical cause of the nonlogarithmic line broadening is due to the explanation given in this work or due to the TLS-TLS interaction as pointed out in Ref. 52. First, it would be interesting to know whether this effect is universal, i.e., whether hole burning on different polymers give identical results: same power law and same crossover time from the logarithmic to the nonlogarithmic (or algebraic) behavior. If this were true, it would hint towards TLS-TLS interaction as the physical cause. Even in this case, however, it would be difficult to argue in favor for this explanation at temperatures above ~ 5 K. It seems so that independently of a possible coherent TLS coupling around 1 K, the explanation given in this work is more intuitive at higher temperatures. Especially, the observation of a transition from (21) and (22) to (23) and (24) would favor this interpretation. Next, elastic measurement up to higher temperatures on exactly the same sample which has been used for the hole burning experiment, i.e., including the chromophore, would also give additional information. Finally, the question how polymer glasses without side chains, like polyethylene (PE) or polybutadiene (PB), behave in hole burning at ultralong time scales seems to be interesting. Following the interpretation of the present work, one would expect no or a later deviation from a logarithmic hole broadening (if σ_0 is sufficiently large) as compared to polymers like PMMA because of the lack of "defects."

V. SUMMARY AND CONCLUSIONS

We have analyzed the energy landscape of glasses containing defects. Specifically, we refer to OH-defects. However, the experimental results on polymers allow to speculate that also some side groups in polymers like the carboxyl group in PMMA may be viewed as a (generalized) defect.

The analysis of LJ glasses has revealed that already small differences between defect and glass dramatically change the energy landscape around this defect, giving rise to additional

extrinsic DWP's. The main characterstics of these extrinsic DWP's are (i) high barrier heights, (ii) high probability that a defect is indeed connected with an extrinsic DWP, (iii) highly localized dynamics around this defect. As already discussed in the Introduction (i) and (ii) are in direct agreement with experimental observations on network-formers. Although the results are derived for a specific model glass we believe that this behaviour may be generic for other types of defect/glass-systems.

This observation allows a straightforward extension of the STM which successfully accounts for the nonlogarithmic dynamics of hole burning experiments on polymer glasses and proteins. In terms of the energy landscape these low temperature experiments mainly probe their fine structure. Comparing the hole burning experiments for polymer glasses and proteins for short times leads to the conclusion that the fine structure is more distinct for polymer glasses. However, the presence of some high energy saddles, corresponding to localized motion, seems to be present in both systems.

ACKNOWLEDGEMENTS

APPENDIX A:

In this Appendix we derive Eq. (20). Starting out from Eq. (17), we first note that

$$
[\epsilon(E,R)/E]P(E,R)\,dEdR = [\epsilon(E,\lambda)/E]P(E,\lambda)\,dEd\lambda
$$
$$
= \left(P_0 e^{-(\lambda-\lambda_0)^2/2\sigma_0^2} + P_1 e^{-(\lambda-\lambda_1)^2/2\sigma_1^2}\right)\,dEd\lambda. \qquad (A.1)
$$

Rewriting Eq. (6) as

$$tR(E, \lambda) = e^{-2[\lambda - \lambda_{\min}(E) - (1/2) \log(tR_{\max}(E))]}, \tag{A.2}$$

we may use the step function approximation for the term $(e^{-t_0 R(E,\lambda)} - e^{-tR(E,\lambda)})$ in Eq. (17),

$$\int_{\lambda_{\min}(E)} d\lambda \left(e^{-t_0 R(E,\lambda)} - e^{-tR(E,\lambda)} \right) \ldots \approx \int_{\xi(E)}^{\lambda_{\min}(E)+(1/2)\log(tR_{\max}(E))} d\lambda \ldots , \tag{A.3}$$

where

$$\xi(E) = \max[\lambda_{\min}(E), \lambda_{\min}(E) + (1/2)\log(t_0 R_{\max}(E))]. \tag{A.4}$$

For a hole burning experiment, we have $t_0 > 1$ s such that at $T \sim O(1)$ K

$$\xi(T) = \lambda_{\min}(T) + (1/2)\log(t_0 R_{\max}(T)) = (1/2)\log(t_0 \widehat{R}(T)), \tag{A.5}$$

where

$$\widehat{R}(E) \equiv R_{\max}(E)e^{2\lambda_{\min}(E)} = KT x \coth x, \tag{A.6}$$

$K = c(\hbar\omega_0/2k_B)^2$ [cf. Eq. (8)]. Note that, due to Eqs. (7) and (8), $\widehat{R}$ depends linearly on temperature. From the first term in Eq. (A.1), we then find with[54]

$$\frac{1}{\sigma\sqrt{2\pi}} \int_{-\infty}^{x} e^{-(y-m)^2/2\sigma^2} dy = \frac{1}{2}\left(1 + \text{erf}\left(\frac{x-m}{\sigma\sqrt{2}}\right)\right), \tag{A.7}$$

where $\text{erf}(z)$ is the error function, that (after setting $\lambda_0 \equiv 0$)

$$\Delta\Gamma^{(1)}(t) = (\pi^2/3\hbar)\langle C\rangle P_0 \int_0^{\infty} dE \ \text{sech}^2(E/2k_BT) \ \times$$
$$\times \ \frac{\sigma_0\sqrt{2\pi}}{2}\left\{\text{erf}\left(\frac{(1/2)\log(t\widehat{R}(E))}{\sigma_0\sqrt{2}}\right) - \text{erf}\left(\frac{\xi(E)}{\sigma_0\sqrt{2}}\right)\right\}. \tag{A.8}$$

From the second term in Eq. (A.1), we find with (A.7) and the definition of the complementary error function $\text{erfc}(z) = 1 + \text{erf}(-z)$ that

$$\Delta\Gamma^{(2)}(t) = (\pi^2/3\hbar)\langle C\rangle P_1 \int_0^{\infty} dE \ \text{sech}^2(E/2k_BT) \ \times$$
$$\times \ \frac{\sigma_1\sqrt{2\pi}}{2}\left\{\text{erfc}\left(\frac{\lambda_1 - (1/2)\log(t\widehat{R}(E))}{\sigma_1\sqrt{2}}\right) - \text{erfc}\left(\frac{\lambda_1 - \xi(E)}{\sigma_1\sqrt{2}}\right)\right\}. \tag{A.9}$$

Upon noting that $\widehat{R}(E)$ is approximately independent of E for $E < 2k_BT$, we find Eq. (20) in the hole burning time regime (A.5).

22

REFERENCES

[1] F. H. Stillinger, Science **267**, 1953 (1995) and references therein.

[2] H. Frauenfelder, G. Petsko, and D. Tsernoglou, Nature (London) **280**, 558 (1979)

[3] A. Ansari, J. Berendzen, S. F. Browne, H. Frauenfelder, I. E. T. Iben, T. B. Sauke, E. Shyamsunder, and R. F. Young, Proc. Natl. Acad. Sci. USA **82**, 5000 (1985).

[4] R. Elber and M. Kaplus, Science **235**, 318 (1987).

[5] H. Frauenfelder, S. G. Sligar, and P. G. Wolynes, Science **254**, 1598 (1991).

[6] H. Frauenfelder and P. G. Wolynes, Physics Today **47**, No. 2, 58 (1994).

[7] D. Thorn Leeson and D. A. Wiersma, Phys. Rev. Lett. **74**, 2138 (1995).

[8] K. Fritsch, J. Friedrich, F. Parak, and J. L. Skinner, Proc. Natl. Acad. Sci. USA **93**, 15141 (1996).

[9] G. P. Singh, H. J. Schink, H. v. Löhneysen, F. Parak, and S. Hunklinger, Z. Phys. B **55**, 23 (1984).

[10] I. E. Iben *et al.*, Phys. Rev. Lett. **62**, 1916 (1989).

[11] K. D. Ball, R. S. Berry, R. E. Kunz, Li Feng-Yen, A. Proykova, D. J. Wales, Science **271**, 963 (1996).

[12] A. Heuer, appears in Phys. Rev. Lett.

[13] P. W. Anderson, B. I. Halperin, and C. M. Varma, Philos. Mag. **25**, 1 (1972).

[14] W. A. Phillips, J. Low Temp. Phys. **7**, 351 (1972).

[15] For a review see: *Amorphous Solids – Low Temperature Properties*, Topics in Current Physics **24**, W. A. Phillips, eds., (Springer, Berlin Heidelberg New York, 1984).

[16] H. Maier and D. Haarer, J. Lumin. **64**, 87 (1995).

[17] H. Maier, B. M. Kharlamov, and D. Haarer, Phys. Rev. Lett. **76**, 2085 (1996).

[18] G. Hannig, Hans Maier, D. Haarer, and B. Kharlamov, Mol. Cryst. Liq. Cryst. **291**, 11 (1996).

[19] J. Gafert, H. Pschierer, and J. Friedrich, Phys. Rev. Lett. **74**, 3704 (1995).

[20] K. Fritsch, A. Eicker, J. Friedrich, B. M. Kharlamov, and J. M. Vanderkooi, submitted to Phys. Rev. Lett.

[21] D. Tielbürger, R. Merz, R. Ehrenfels, and S. Hunklinger; Phys. Rev. B **45**, 2750 (1992).

[22] S. Rau, C. Enss, S. Hunklinger, P. Neu, and A. Würger, Phys. Rev. B **52**, 7179 (1995).

[23] K. A. Topp and D. G. Cahill, Z. Phys. B **101**, 235 (1996).

[24] C. R. Kurkjian and J. T. Krause, J. Am. Ceram. Soc. **49**, 171 (1969).

[25] W. A. Phillips, Phil. Mag. B **43**, 747 (1981).

[26] J. M. Crissman, J. A. Sauer, and A. E. Woodward, J. Polymer Sci. **A2**, 5075 (1964).

[27] J. Heijboer and M. Pineri, in *Nonmetallic Materials and Composites at Low Temperatures*, Vol. 2, G. Hartwig and D. Evans, eds., (Plenum Press, New York, 1982), p. 89-116.

[28] G. Hartwig and G. Schwarz, in *Nonmetallic Materials and Composites at Low Temperatures*, Vol. 3, G. Hartwig and D. Evans, eds., (Plenum Press, New York, 1986), p. 117-126.

[29] N. Geis, G. Kaspar, and S. Hunklinger, in *Nonmetallic Materials and Composites at Low Temperatures*, Vol. 3, G. Hartwig and D. Evans, eds., (Plenum Press, New York, 1986), p. 99-105.

[30] A. Nittke, M. Scherl, P. Esqinazi, W. Lorenz, Junyun Li, and Frank Pobell, J. Low. Temp. Phys. **98**, 517 (1995).

[31] K. Schmidt-Rohr et al., Macromolecules **27**, 4733, (1994).

[32] A. Heuer and R. J. Silbey, Phys. Rev. B **53**, 609 (1996).

[33] T. A. Weber and F. H. Stillinger, Phys. Rev. B **32**, 5402 (1985).

[34] A. Heuer and R. J. Silbey, Phys. Rev. B **48**, 9411 (1993).

[35] R. Jankowiak and G. J. Small, Science **237**, 618 (1987).

[36] We want to mention that although this formula (12) is sufficient for all practical purposes, the relaxation process itself is not classical for the high barriers needed in the temperature regime of the absorption peak. Instead, relaxation occurs via direct tunneling from many excited levels of the DWP and intra-well vibrational transitions between theses states. The Arrhenius rate (12) has to be seen as an effective rate whose exponential temperature dependence arises from transitions between different vibrational levels of each well via the Orbach process. See P. Neu and A. Heuer, J. Chem. Phys., **106**, 1749 (1997) for more details.

[37] K. S. Gilroy and W. A. Phillips, Phil. Mag. B **43**, 735 (1981).

[38] G. Federle and S. Hunklinger, J. de Physique, C9 (12), Tome 43, p. C9-505 (1982).

[39] Noting that at $\omega = 2\pi \times 15$ MHz the peak temperature lies at $T_{\max} \approx 12$ K,[38] the relation $V_{\max} = -k_B T_{\max} \log(\omega \tau_0)$ (cf. Eq. (2.105) in Ref. 22) with $\tau_0 = 10^{-13}$ s provides an estimation $V_{\max}(\text{PMMA}) \approx 220$ K. Using the same formula to calculate $T_{\max}$ at $\omega = 2\pi \times 535$ Hz with this value of $V_{\max}$ gives an expected peak temperature of ~ 10 K. Comparing this with the data of Fig. 12 in Ref. 30, one clearly sees that this peak temperature is too low to separate the relaxation peak from the plateau.

[40] W. Köhler, J. Friedrich, and H. Scheer, Phys. Rev. A **37**, 660 (1988).

[41] P. Schellenberg and J. Friedrich, in *Disorder Effects on Relaxational Processes*, edited by D. Richter and A. Blumen (Springer, Berlin Heidelberg, 1994).

[42] T. S. Bai and M. D. Fayer, Phys. Rev. B **39**, 11066 (1989).

[43] R. Wannemacher, J. M. A. Koedijk, and S. Völker, Chem. Phys. Lett. **206**, 1 (1993).

[44] S. Völker, in *Relaxation Processes in Molecular Excited States*, Series C: Molecular Structures, edited by J. Fünfschilling (Kluwer Academic Press, 1989).

[45] P. Hu and L. R. Walker, Phys. Rev. B **18**, 1300 (1978).

[46] J. L. Black and B. I. Halperin, Phys. Rev. B **16**, 2879 (1977).

[47] T. L. Reinecke, Solid State Commun. **32**, 1103 (1979).

[48] A. Suarez and R. J. Silbey, Chem. Phys. Lett. **218**, 445 (1994).

[49] C. C. Yu and A. J. Leggett, Comments Condensed Matter Phys. **14**, 231 (1991).

[50] S. N. Coppersmith, Phys. Rev. Lett. **67**, 2315 (1991).

[51] A. L. Burin and Yu. Kagan, JETP **80**, 761 (1995).

[52] P. Neu, D. R. Reichman, and R. J. Silbey, appears in Phys. Rev. B.

[53] K. Zemke, K. Schmidt-Rohr, H. W. Spiess, Acta Polymer. **45**, 148 (1994).

[54] M. Abromowitz, I A. Stegun, *Pocketbook of Mathematical Functions*, Verlag Harri Deutsch (1984).

Figure captions

FIG. 1. The probability to find extrinsic and intrinsic DWP's by our search algorithm. As discussed in the text the probability for intrinsic DWP's has been scaled such that for $\alpha = 1$ both probabilities agree. The observation that no extrinsic DWP's have been found for $\alpha = 0.7$ is indicated by the arrow. Note the logarithmic scale for the probability.

FIG. 2. The average effective mass p in dependence of α.

FIG. 3. The distribution of potential heights for $\alpha = 1.0$ and $\alpha = 1.6$.

FIG. 4. The average potential height V in dependence of α.

FIG. 5. The average deformation potential γ in dependence of α. The data have been normalized such that $\gamma(\alpha = 1) = 1$.

FIG. 6. Internal friction, Q^{-1}, of the OH-doped network glass a-B_2O_3. The data are from Ref. 22. The solid line is a fit with the distribution (9); the dashed line line shows the contribution of the internal DWP's. The parameters are $C \equiv P_0\gamma^2/\varrho v^2 = 3.6 \times 10^{-4}$, $E_0/k_B = 18$ K, $\tilde{\sigma}_0 = 450$ K, $P_0/P_1 = 0.22$, $V_1 = 2000$ K, and $\tilde{\sigma}_1 = 900$ K.

FIG. 7. Hole broadening in the polymer glass PMMA at 2 K (upper curve), 1 K (middle curve), and 0.5 K (lower curve). The experimental data are from Ref. 17,18. The solid lines are fits with Eq. (20) with parameters given in Table I; the dashed line depicts the contribution of the first term, the dash-dotted line the contribution of the second term in Eq. (20). A nearly algebraic line broadening between $10^2 - 10^4$ min emerges from the superposition of both terms.

FIG. 8. Hole broadening in glycerol/water glass (upper curve) and the protein myoglobin (lower curve). The experimental data are from Ref. 19. The solid and dashed line are fits with Eq. (20) with parameters given in Table I and II. The protein data have been fitted without a $\log(t)$-term ($P_0 = 0$).

FIG. 9. Hole broadening in the protein cytochrome c. The experimental data are from Ref. 20; time between cooling and burning: 94 min ($+$), 4398 min ($\circ$), and 10093 min ($*$). The full and dashed line are fits with Eq. (20) with both terms (full line) and only the second term (dashed line). Parameters given in Table I and II. The dash-dotted line depicts a

27

possible contribution of a $\log(t)$-term.

<center>**Tables**</center>

Table I: Parameters for PMMA, glycerol/water glass and cytochrome (intrinsic + extrinsic DWP's):

	λ_1	σ_0	σ_1	P_1/P_0	$P_0\langle C\rangle$	K [K^{-1}s^{-1}]
PMMA	20	30	$\sqrt{1.3}$	8	0.95×10^{-5}	5×10^{11}
glycerol/water	20	20	$\sqrt{1.7}$	28	3.49×10^{-5}	3.55×10^{11}
cytochrome	19.7	20	1	50	0.35×10^{-5}	4.1×10^{10}

Table II: Parameters for myoglobin and cytochrome (extrinsic DWP's):

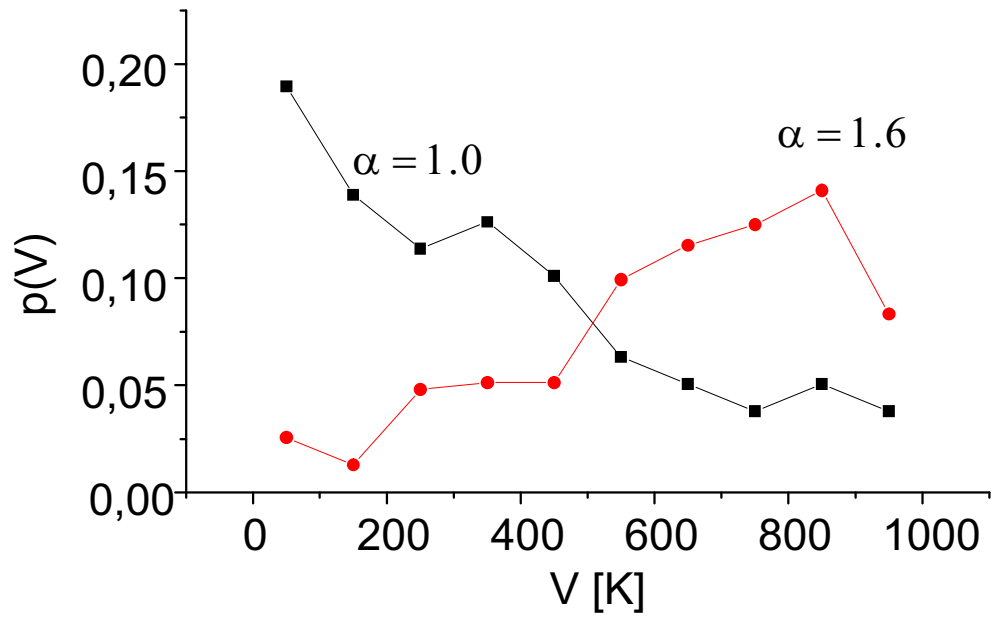|	λ_1	σ_1	P_0	$P_1\langle C\rangle$	K [K^{-1}s^{-1}]
myoglobin	20	$\sqrt{3}$	0	62.4×10^{-5}	6.6×10^{10}
cytochrome	19.7	1	0	17.3×10^{-5}	4.1×10^{10}

<center>28</center>
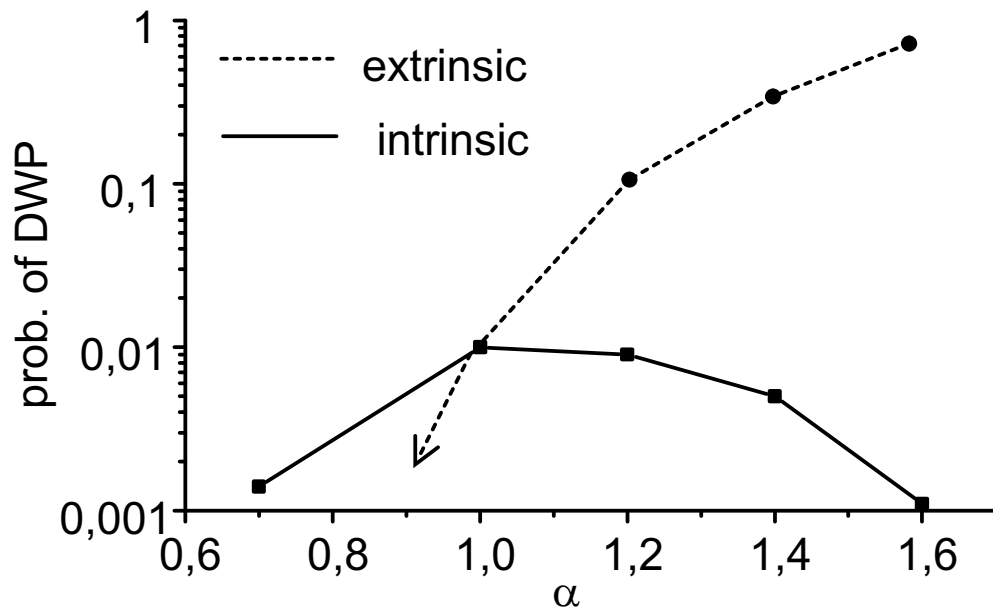
FIG. 1: Heuer et al.

FIG. 2: Heuer et al.
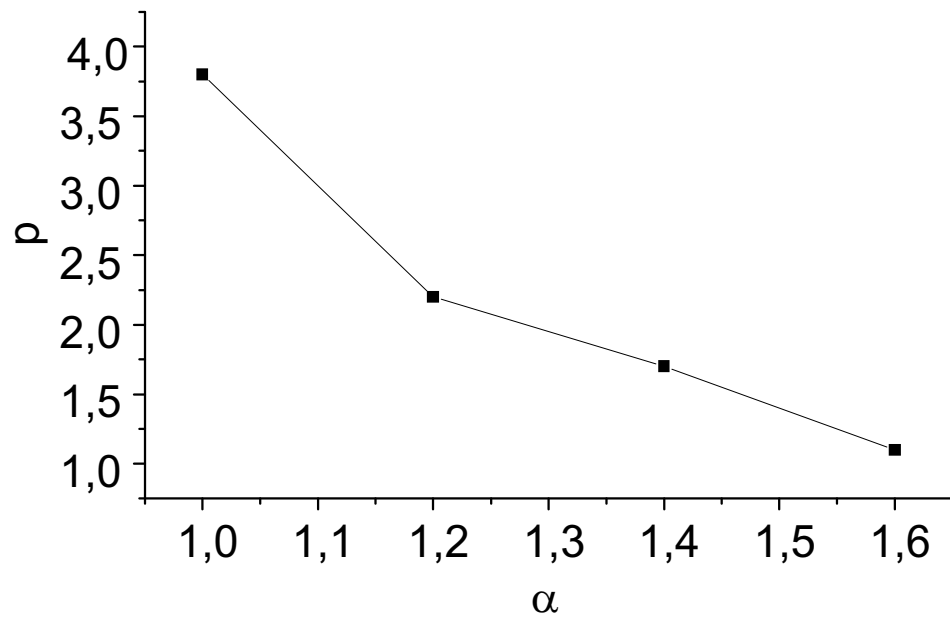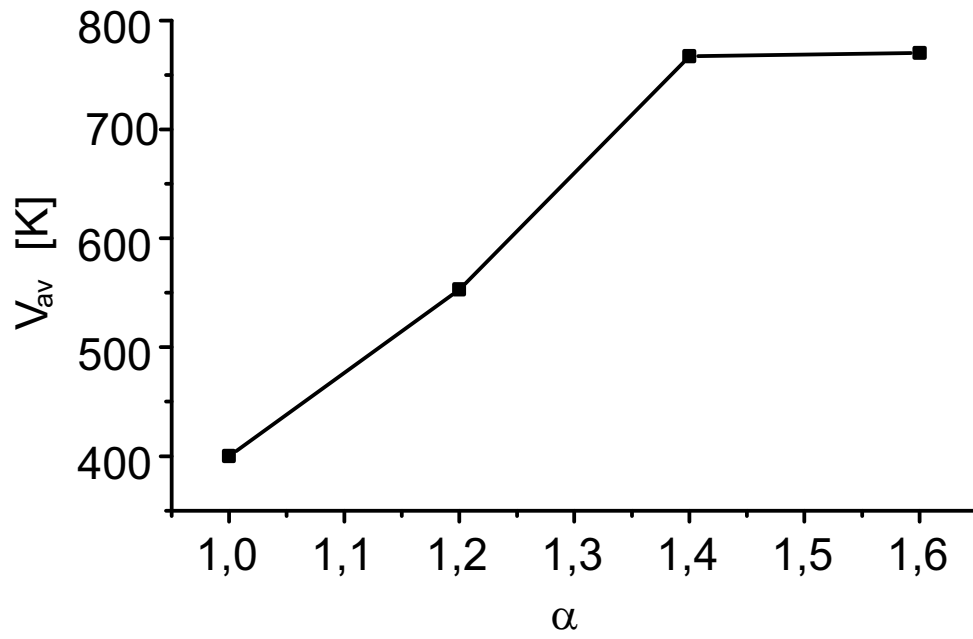
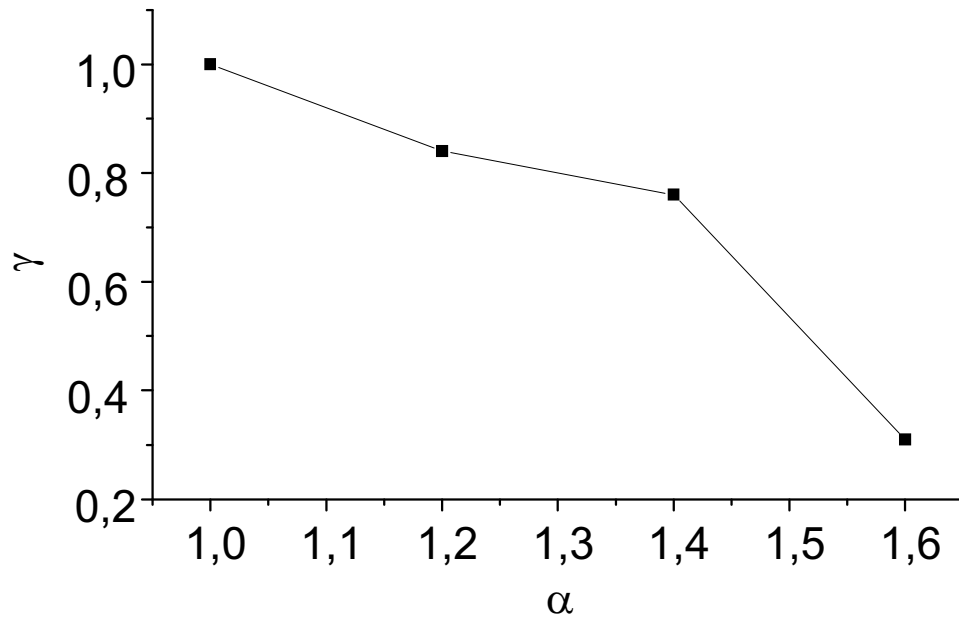FIG. 3: Heuer et al.

FIG. 4: Heuer et al.

FIG. 5: Heuer et al.
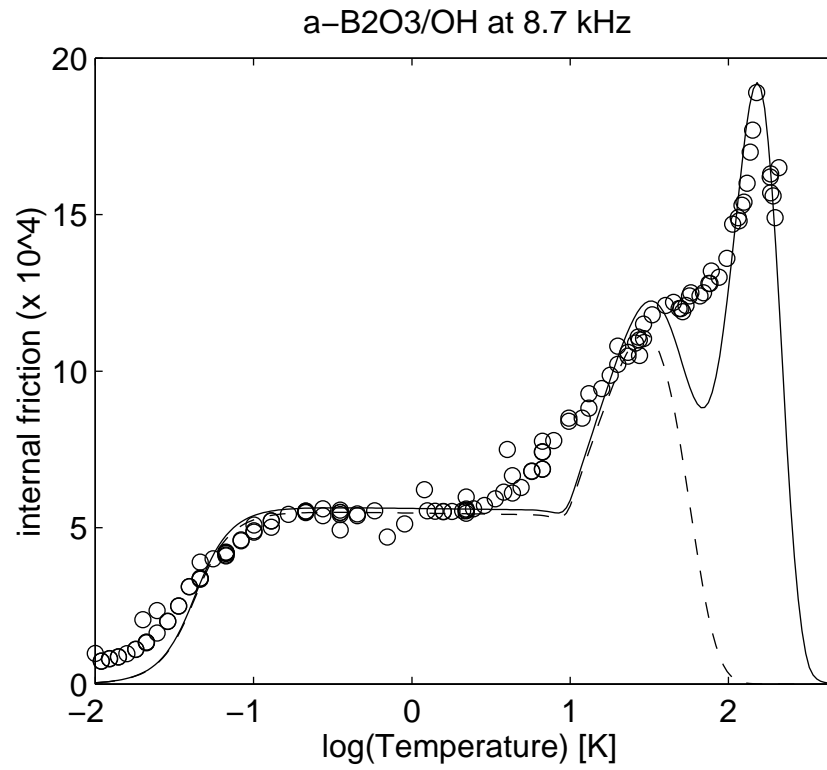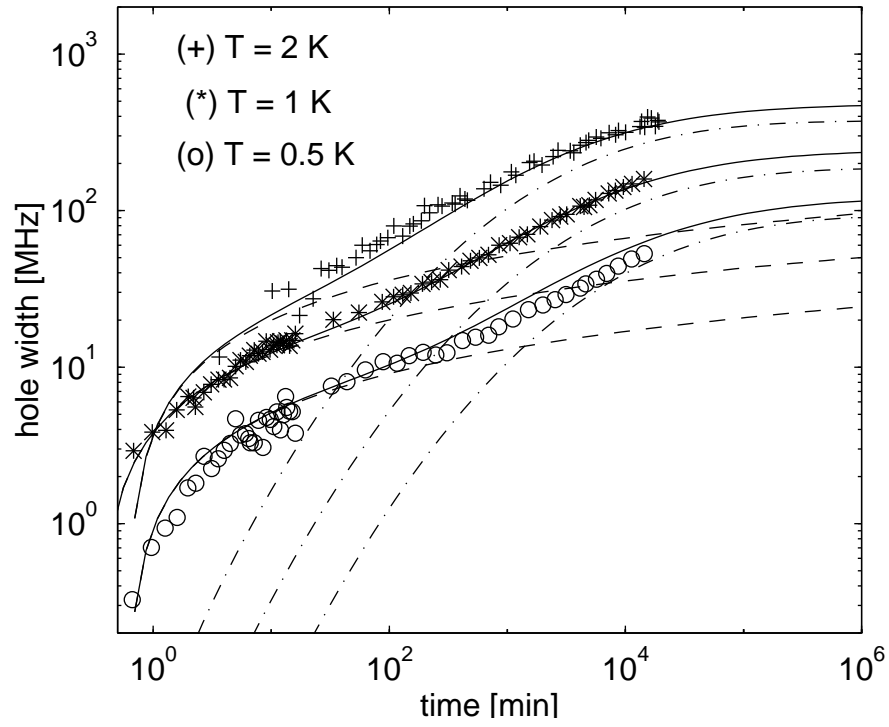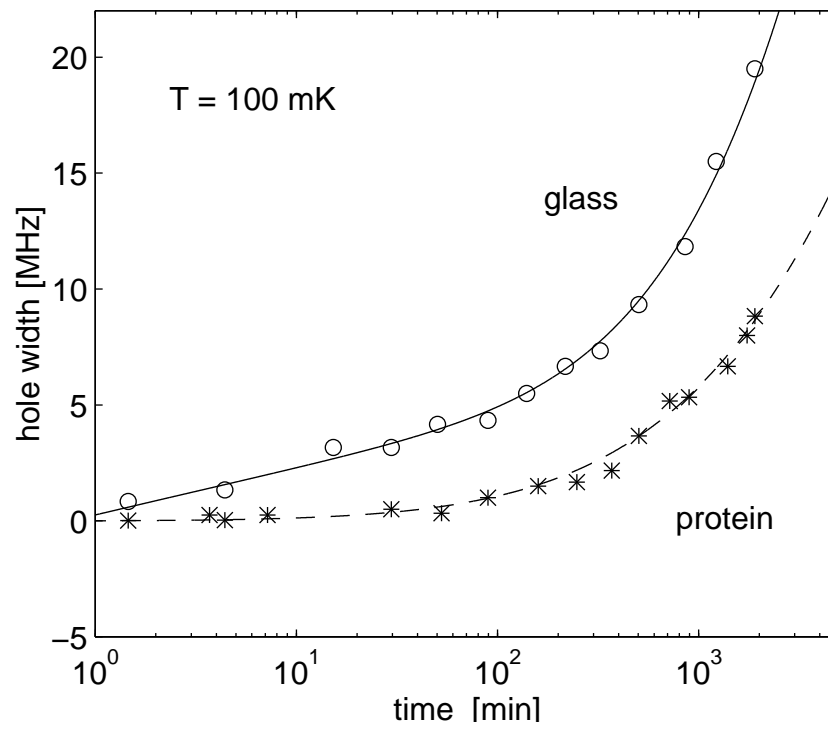

FIG. 6: Heuer et al.

a−B2O3/OH at 8.7 kHz

FIG. 7: Heu

FIG. 8: Heuer et al.

FIG. 9: Heuer et al.